Journal of Ultrafine Grained and Nanostructured Materials
https://jufgnsm.ut.ac.ir
Vol. 56, No.2, December 2023, pp. 129-136
Print ISSN: 2423-6845 Online ISSN: 2423-6837
DOI: 10.22059/jufgnsm.2023.02.01

Photocatalytic performance of SnS_2 nanoflakes synthesized through a facile reflux method

Amir Saadati[1], Saeed Sheibani[1,*]

[1]School of Metallurgy and Materials Engineering, College of Engineering, University of Tehran, Tehran, Iran;

Recieved: 1 June 2023; Accepted: 30 June 2023

**Corresponding author email: ssheibani@ut.ac.ir*

ABSTRACT

Developing an effective yet convenient synthesis method to achieve visible light-responsive metal sulfides has been one of the main challenges in the photocatalysis field. In this study, a facile reflux approach has been proposed to synthesize SnS_2 nanoflakes for photocatalytic degradation of methylene blue (MB) as an organic pollutant. X-ray diffraction (XRD) pattern and Raman spectroscopy confirmed the formation of SnS_2 with a hexagonal crystal structure. The results of the nitrogen (N_2) adsorption-desorption were analyzed by Brunauer-Emmett-Teller (BET) and Barrett-Joyner-Halenda (BJH) methods. BET results exhibited specific surface area, total pore volume, and average pore diameter of 84 m^2/g, 0.2 cm^3/g, and 10 nm, respectively. The BJH outcomes indicated a distribution of about 40 nm for pore size with a peak of about 2 nm. The nanoflake morphology and band gap energy of approximately 2.15 eV were revealed through field emission electron microscope (FESEM) and diffuse reflectance spectroscopy (DRS), proving the successful synthesis of visible light-responsive SnS2 nanoflakes. The efficiency of MB photodegradation over SnS_2 nanoflakes was 78% under visible light radiation. The photocatalytic reaction followed a pseudo-first-order kinetic model with the calculated rate constant of 0.0045 min^{-1}. Additionally, the photocatalytic degradation mechanism over SnS_2 nanoflakes was investigated, and the results proved the successful contribution of holes and hydroxyl radicals in the mineralization of MB.

Keywords: *Reflux; SnS_2; Nanoflakes; Photocatalysis; Degradation.*

1. Introduction

Organic dyes have become one of the main sources of pollution in water. Wastewater consisting of these pollutants can put all forms of life in danger; thus, exploring highly efficient methods to deal with such phenomena is of great importance. Different types of strategies have been employed to treat polluted water, including biochemical oxidation, sedimentation, and precipitation, as biological, physical, and chemical approaches, respectively. These methods cannot completely mineralize the organic pollutants [1–3]. Recently, photocatalysis has attracted considerable attention due to the mild condition, capability of complete mineralization of pollutants, and use of sunlight as the energy input [4,5]. However, developing highly efficient semiconductors to employ as a photocatalyst is still challenging. Proper band gap energy is one of the primary characteristics that should be taken into account to harvest visible light from sunlight [6,7].

Among various semiconductors, metal sulfides such as SnS_2, CdS, Ag_2S possess narrow band

gap energy, which makes visible light absorption feasible. Moreover, the low cost and relatively high chemical stability of sulfides can introduce these types of semiconductors as potent candidates for photocatalytic applications [8]. Among metal sulfides, SnS_2 has been employed extensively compared to other metal sulfides due mainly to its higher stability and nontoxic nature. However, high bulk recombination of electron-hole pairs after excitation restricts further usage of this semiconductor in the photocatalysis field. Different strategies have been taken into consideration to overcome such a drawback, namely heterostructure formation, doping, and morphological engineering. Among these approaches, morphological engineering has been highlighted to achieve various properties in a single material [9–11].

The reflux method has been introduced as one of the most effective synthesis strategies to achieve different morphology by making alterations in the sequence of adding precursors or changing the solvent. Zhang et al. [12] investigated the effect of synthesis parameters such as temperature, type of solvent, and adding sequence on the properties of SnS_2. Nanoparticles, nanoflowers, and nanosheets were the obtained morphologies, signifying the flexible nature of the reflux method to achieve different types of morphology. The reaction temperature was also reported to have a profound impact on the morphology of SnS_2, modifying the morphology from nanoparticles to nanosheets [13].

According to our knowledge, reducing the migration distance of electron-hole pairs in SnS_2 through nanoflake or nanosheet synthesis can improve the drawbacks of this metal sulfide, and introducing a convenient method for synthesis is crucial. Hydrothermal has been reported as a common synthesis strategy to achieve such nanostructure morphology [14,15]. However, expensive equipment, high temperature, and time-consuming are disadvantages that restrict the versatile use of this synthesis method.

In this research, a facile and relatively low-temperature synthesis method, reflux, has been introduced to achieve nanoflake structure in SnS_2 powder. The selected reflux time was lower than the previous reports to reduce the migration distance of electron-hole pairs by achieving fine morphology. Not only could this phenomenon affect the separation behavior, but it could also promote organic pollutants' adsorption on the surface of this metal sulfide. Several characterization methods were also employed to investigate the properties of the synthesized SnS_2 nanoflakes. Also, the capability of synthesized su SnS_2 in the photocatalytic degradation of pollutant in aqueous solution has been investigated.

2. Experimental procedure

2.1. Synthesis

All the materials were analytical grades and employed without further purification. Distilled water and absolute ethanol were used for washing during synthesis. SnS_2 nanoflakes have been synthesized through a convenient reflux method. The synthesis process began with tin (IV) chloride pentahydrate dissolution in 30 mL ethylene glycol, after which the solution was transferred to a three-neck flask with 250 mL volume. The flask was equipped with an injection system, condenser, and thermometer. The same procedure was done for the thioacetamide solution (molar ratio of 4 with respect to the tin (IV) chloride pentahydrate solution) and then transferred to the injection system. Then, the flask with its equipment was put in an oil bath to begin the heating program. First, the tin (IV) chloride pentahydrate solution was stirred in the oil bath with 7 ˚C/min heating rate. After that, the thioacetamide solution was injected once the temperature reached 160 ˚C, and then the stirring process continued until 60 min. Eventually, the flask was removed from the oil bath to let the suspension cool down. Centrifugation, washing with distilled water and absolute ethanol, and drying were the additional steps to achieve SnS_2 powder.

2.2. Characterizations

The crystallographic properties of the synthesized samples were examined using a Phillips-PW3040/60 X-ray diffractometer, with the X-ray source being Cu K_α with a wavelength of 1.54 Å. The raman spectrum of the sample was recorded by means of a Jobin-Yvon model equipped with a 532 nm laser. The specific surface area of the sample was determined using the BET method on a BELSORP Mini II instrument, through which N_2 was used as the adsorbate at a temperature of 77 K. The morphology of the photocatalysts in their initial state was investigated using a CamScanMV2300 FESEM equipped with a JEOL Centurio energy-dispersive spectroscopy (EDS). The optical characteristics of the photocatalysts were assessed through DRS using the Shimadzu MPC-2200 instrument. A conventional three-

electrode system (the counter electrode was a 2 mm diameter platinum disk, the reference electrode was a calomel electrode, and the working electrode was 2 mm diameter glassy carbon coated with SnS2) was utilized for Mott-Schottky analysis with 500 Hz frequency, 10 mV amplitude, and in 10 mL Na_2SO_4 (0.2 M). The working electrode was prepared following a specific procedure: initially, 3 mg of photocatalysts were dispersed in 100 µL of ethanol through sonication for 10 min. Next, 3 µL of the resulting suspension was carefully applied onto the surface of the glassy carbon electrode and subsequently dried under IR lamp radiation. Finally, a Nafion solution with a volume of 1 µL was added to the dried electrode and dried once again using the same method.

2.3. Photocatalytic experiment

The photocatalytic performance of the synthesized SnS_2 nanoflake was thoroughly investigated in terms of its capability to degrade MB, as an organic pollutant, under visible light radiation. To conduct the experiment, a dosage of 0.067 g/L (equivalent to 10 mg of photocatalyst in a 150 mL solution of MB) was utilized. For the illumination source, an Orsam visible light system with a power output of 150 W was employed, complemented by the use of an ultraviolet (UV) cutoff filter. The suspension of the photocatalyst and MB solution underwent a dark period of 60 min, allowing for the attainment of equilibrium through adsorption and desorption processes. This ensured that the system reached a stable state prior to the visible light exposure. During the photocatalytic test, multiple samples were collected at 30 min intervals over a period of 180 min. 2 mL of each sample was extracted and subjected to centrifugation to analyze the concentration of MB. Subsequently, the MB concentration was determined using a UNICO 2100 UV-visible (UV-vis) spectrophotometer, with measurements conducted at a specific wavelength of 664 nm. Additionally, a blank test was also conducted to establish a reference point. In this control experiment, the MB solution was subjected to visible light irradiation without the presence of any photocatalysts. Finally, the photodegradation process of MB over SnS_2 nanoflakes was kinetically evaluated employing a pseudo-first-order kinetic model (Eq. 1):

$$ln\frac{C_0}{C_t} = kt \quad (1)$$

In this equation, C_0 and C_t are the initial concentration and concentration at time t, respectively. k is the pseudo-first-order rate constant of the photodegradation process, and t is the time.

3. Results and discussion

Fig. 1 exhibited the XRD pattern and Raman graph of the synthesized SnS2 nanoflakes. As shown in Fig. 1 (a), the XRD pattern of the sample possessed 6 main diffraction peaks within the 2θ range of 10-70°. Firstly, the peak broadening phenomenon in the XRD graphs confirmed the nanostructure nature of the as-synthesized sample. Secondly, according to the JCPDS No. 23-0677 reference card, these characteristic peaks were consistent with the hexagonal crystal structure of the nanoflakes [13]. Thirdly, these peaks were located at the 2θ values of 14.98, 28.48, 32.74, 50.00, 52.54, and 60.82 °, which could be indexed to the Miller indices of (001), (100), (101), (110), (111), and (201), respectively.

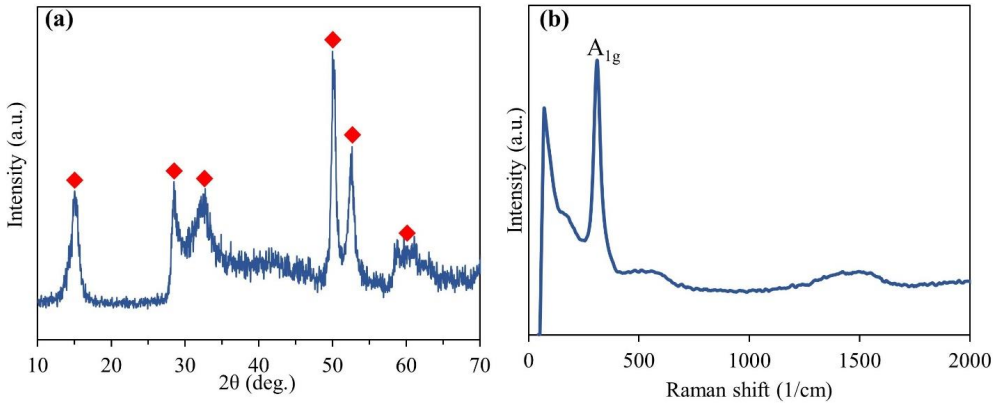

Fig. 1- (a) XRD pattern and (b) Raman spectrum of the synthesized SnS_2 nanoflakes.

Finally, there were no peaks related to the impurity phase or byproducts in the synthesized SnS2 nanoflakes, indicating the capability of the reflux method to synthesize nanostructure powder with high purity [16]. Besides, the Raman spectrum of the nanoflakes was brought in Fig. 1 (b). The strong and sharp peak at the Raman shift of approximately 312 cm^{-1} confirmed the successful synthesis of SnS_2. This peak could be attributed to the out of plane A_{1g} vibration mode of the hexagonal crystal structure of the SnS2 nanoflakes, which was in agreement with the XRD pattern [17].

To evaluate the textural properties of the synthesized sample, including specific surface area, pore volume, and pore size distribution, the N_2 adsorption-desorption method was employed. Then, the data were analyzed utilizing BET and BJH models to investigate the as-mentioned properties. Fig. 2 (a) exhibited the obtained N_2 adsorption-desorption branches of the SnS_2 nanoflakes, demonstrating a type IV isotherm. This type of isotherm could prove that the synthesized nanoflakes mainly possessed mesoporous structures with pore sizes within the range of 2-50 nm [18]. According to the International Union of Pure and Applied Chemistry (IUPAC), this type of hysteresis loop can be classified as an H3 hysteresis loop, confirming no limitation in adsorption at high P/P_0 [19]. This characteristic could yield the result that the as-synthesized sample consisted of plate-like morphology, which will further discuss by FESEM images of the sample. The calculated specific surface area, total pore volume, and mean pore diameter were 84 m^2/g, 0.2 cm^3/g, and 10 nm, respectively. The pore size distribution was also brought in Fig. 2 (b), indicating a size distribution below 40 nm. BJH analysis confirmed that the peak of this distribution was centered at approximately 2 nm. Therefore, BET and BJH evaluations revealed that the synthesized SnS_2 could be a potent candidate to catalyze the photodegradation process of organic dyes in terms of textural properties. Generally, the surface of a semiconductor plays a prominent role in triggering photocatalytic reactions by the adsorption of pollutants, indicating that improved textural properties are of great importance [20]. The synthesized SnS_2 exhibited suitable conditions for improved adsorption properties as the obtained specific surface area and pore properties could facilitate organic dye adsorption and, thus, photocatalytic reactions.

The morphology of the as-synthesized SnS_2 was assessed, and the resulting FESEM images were displayed in Fig. 3. As shown in Fig. 3 (a), there were some areas where the thickness of the nanoparticles was extremely lower than the other two dimensions, which might draw a conclusion that the synthesized SnS_2 consisted of nanoflake morphology with consistent diameters. The observed morphology was in accordance with the obtained isotherm branches in the BET results. Plus, higher FESEM magnification in Fig. 3 (b) gained more valuable information about the synthesized sample. Within this image, it could be observed the as-mentioned morphology, especially in the marked area, with an approximate diameter of 35 nm. Fig. 3 (b) also shows the marked area, from which elemental mapping images were obtained. The mapping images within the marked area demonstrated the uniform distribution of Sn and S atoms throughout the SnS2 nanoflakes (Fig. 3 (c), (d), and (e)). These results provided further evidence that the synthesized SnS_2 through the reflux method possessed high purity without any detectable impurities.

The optical properties of SnS2 were investigated employing UV-Vis DRS spectroscopy, and the

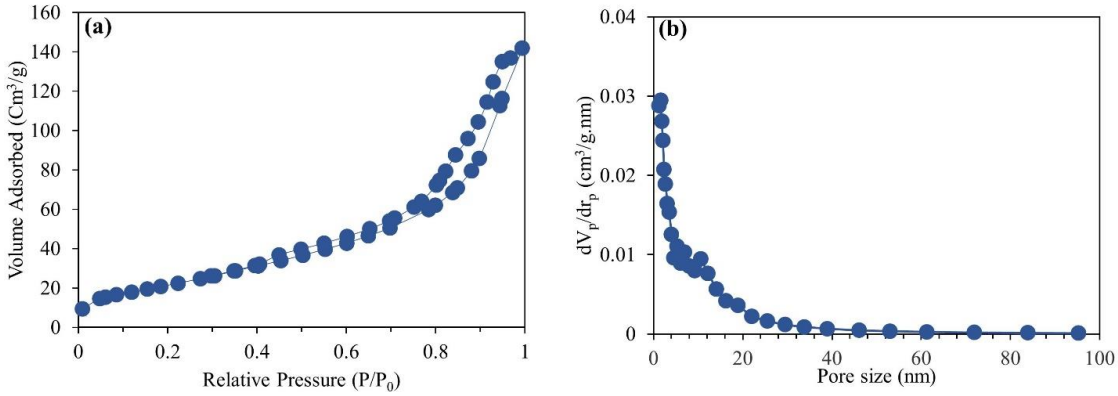

Fig. 2- (a) N_2 adsorption-desorption branches and (b) pore size distribution of the SnS_2 nanoflakes.

obtained absorbance versus wavelength with the corresponding Tauc plot were brought in Fig. 4. As shown in Fig. 4 (a), the synthesized SnS_2 nanoflakes exhibited relatively strong absorption in the visible light region with an absorption edge of approximately 600 nm. Hence, these results could prove the visible light-responsive nature of the as-synthesized sample through the reflux method. Tauc equation (Eq. 2) was employed to calculate the band gap energy of the sample. Since SnS_2 possesses direct band gap energy, the equation was as follows [21,22]:

$$(\alpha h\nu)^2 = A(h\nu - E_g) \quad (2)$$

In Eq. 2, the variables E_g, ν, h, A, and α represent different quantities. Eg corresponds to the band gap energy, ν represents the frequency of vibrations, h denotes the Planck constant, A signifies a constant, and α represents the absorption coefficient. The result of $(\alpha h\nu)^2$ versus hν plot in Fig. 4 (b) was used for band gap energy calculation. By extending the linear portion of the plot to intersect the x-axis (abscissa), the optical band gap energy was determined. The calculated band gap energy of the SnS2 nanoflakes was approximately 2.15 eV, which was comparable to those values reported in the literature. Generally, there is a negative correlation between band gap energy and particle size of a semiconductor, and the reported band gap energy of SnS_2 is in the range of 2-2.53 eV [12,23]. The obtained band gap energy of SnS2

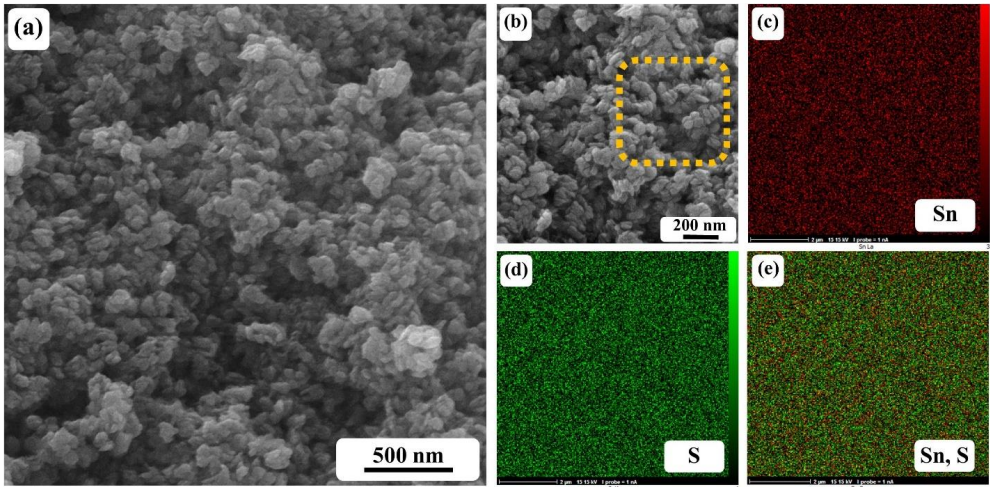

Fig. 3- (a) FESEM image, (b) higher magnification image, (c) Sn, (d) S, and (e) Sn and S mapping images (of the marked area in (b)) of the synthesized SnS_2 nanoflakes.

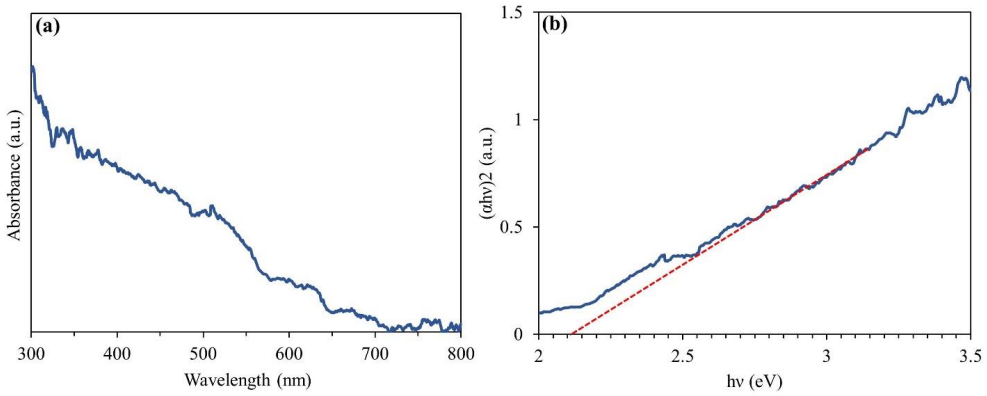

Fig. 4- (a) UV-Vis DRS spectrum with the corresponding (b) Tauc plot of the synthesized SnS_2.

with an approximate size of 35 nm was slightly higher than the band gap value of SnS2 with larger particle size in other research. Park et al. [24] synthesized a series of SnS_2 nanostructures through a microwave-assisted method. The obtained band gap energies varied from 2.02 to 2.05 eV. Zhang et al. [25] also reported a size-controlled hydrothermal method through which band gap energies of about 2.12-2.23 eV were achieved.

The effectiveness of the synthesized SnS2 nanoflakes in photocatalytic activity under visible light exposure was assessed using a 2 mg/L solution of MB, and the results were illustrated in Fig. 5. The removal efficiency of MB, in the presence of the SnS2 sample, was reported based on the heterogenous photocatalysis definition, which considers adsorption as one of the contributing steps [26]. As exhibited in Fig. 5 (a), the blank test outcomes demonstrated that MB degradation was minimal in the absence of a photocatalyst under visible light radiation. However, considerable improvement in the adsorption and photodegradation of MB was observed in the presence of SnS_2 nanoflakes as the photocatalyst. The photocatalytic efficiency of SnS_2 nanoflakes towards MB degradation was 73%, indicating the high capability of the synthesized sample in photocatalytic applications. Furthermore, the pseudo-first-order fitting results were shown in Fig. 5 (b). As illustrated, the obtained rate constant for photodegradation of MB in the presence of SnS_2 was 0.0045 min^{-1}. The results from the photocatalytic degradation of MB confirmed that the visible light-responsive SnS_2 could readily trigger photocatalytic reactions. Moreover, the obtained efficiency was comparable to the values reported by other research groups [27,28]. Qiang et al. [29] employed a hydrothermal method for SnS_2 synthesis, and the reported efficiency towards MB photodegradation was only 44%. In another work, Govindan et al. [30] reported a two-step sol-gel-assisted microwave synthesis approach to synthesize flower-like SnS_2, and the obtained MB photodegradation efficiency was approximately 70%. Hence, these comparisons provided evidence to the fact that the proposed reflux method was highly capable of synthesizing SnS_2 nanostructures.

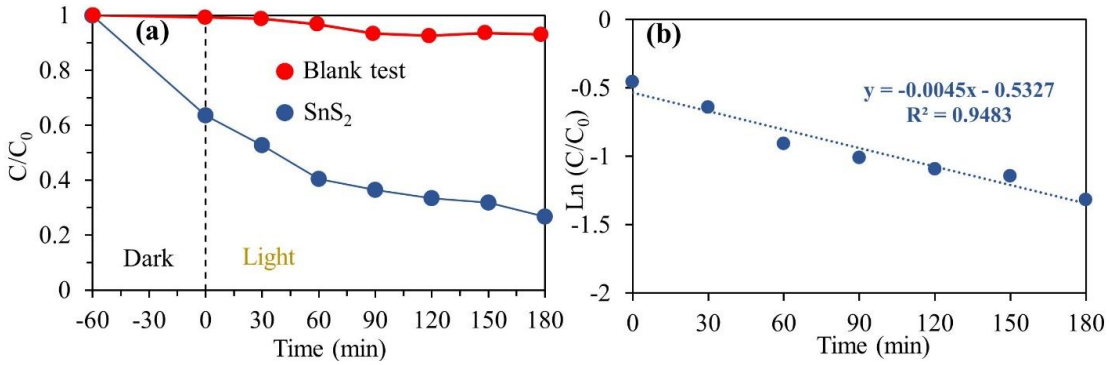

Fig. 5- (a) C/C0 vs. time plot of MB photodegradation over SnS_2 nanoflakes. (b) the fitting results by employing the pseudo-first-order equation.

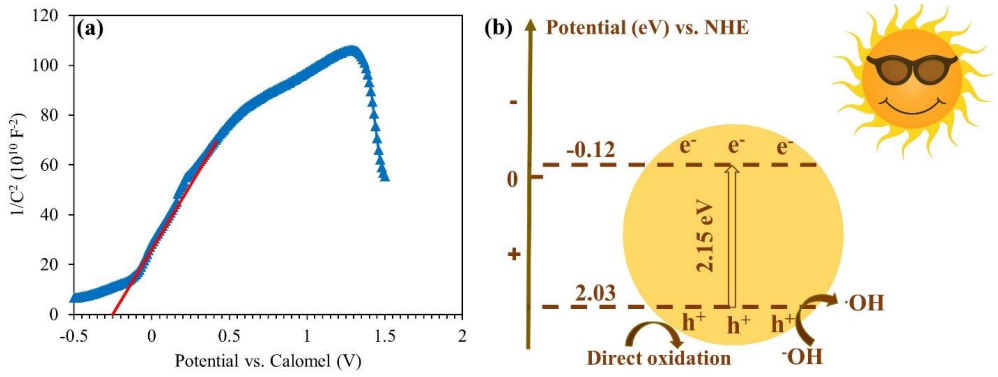

Fig. 6- a) Mott-Schottky plot of the synthesized SnS_2 nanoflakes and (b) the schematic representation of active species generation over SnS_2 nanoflakes.

The Mott-Schottky plot of the SnS_2 nanoflakes was obtained to gain deeper insights into the characteristics of the semiconductor, including its type, flat band potential, and band positions. Fig. 6 (a) depicted the $1/C^2$ vs. V (vs. calomel) plot of the nanoflakes. As observed, the positive slope in the linear region of the curve indicated that the synthesized SnS_2 was an n-type semiconductor with electrons serving as the primary charge carriers [31]. By extrapolating the linear region of the curve and determining the x-intercept, the flat band potential of the photocatalyst was calculated [32]. With respect to the calomel reference electrode, the calculated flat band potential of SnS_2 nanoflakes was -0.26 eV, which could be converted to the normal hydrogen electrode (NHE) as the reference. The calculated flat band potential with respect to NHE was -0.02 eV. Additionally, the bottom of the conduction band for n-type semiconductors is typically more negative than the corresponding flat band potentials by approximately -0.1 V [33]. Based on this information, the conduction band potential of SnS_2 was estimated to be -0.12 eV. The valence band potential was also determined by using the estimated conduction band and band gap energy obtained from the DRS result. Accordingly, the valence band position of SnS2 was found to be 2.03 eV. All the mentioned calculations were summarized in the schematic band structure of SnS_2 in Fig. 6 (b) to investigate the photodegradation mechanism. As demonstrated, electron-hole pairs could create after visible light irradiation (Eq. 3), after which the photogenerated hole could contribute directly to the oxidation process of MB (Eq. 4). Moreover, the holes could produce hydroxyl radicals since the valence band potential was more positive than the required potential for hydroxyl radical formation (1.99 eV vs. NHE) [34]. The produced hydroxyl radicals could also have a prominent role in MB photodegradation (Eqs. 5 and 6). It was worth mentioning that the photogenerated electrons did not possess enough potential to generate superoxide radicals (-0.33 eV vs. NHE) [21].

$$SnS_2 + h\nu \rightarrow SnS_2\,(e^-, h^+) \quad (1)$$

$$MB + h^+ \rightarrow \text{intermediates} \rightarrow \text{mineralization} \quad (2)$$

$$h^+ + {}^-OH \rightarrow {}^{\cdot}OH \quad (3)$$

$$MB + {}^{\cdot}OH \rightarrow \text{intermediates} \rightarrow \text{mineralization} \quad (4)$$

4. Conclusions

In conclusion, SnS2 nanoflakes were synthesized employing a facile reflux method to achieve a visible light-responsive photocatalyst. Several characterization methods have been utilized to investigate the properties of the as-synthesized sample. XRD and Raman spectroscopy results demonstrated the successful synthesis of SnS2 nanostructure with the hexagonal crystal structure. The synthesized SnS2 nanoflakes exhibited specific surface areas of 84 m2/g and a mean pore size diameter of about 10 nm, suggesting proper textural properties for photocatalytic applications. Moreover, the nanoflake morphology with a uniform chemical composition of the sample was revealed by employing FESEM and elemental mapping images. SnS2 nanoflakes showed an absorption edge and bang gap energy of approximately 600 nm and 2.15 eV, respectively. Finally, the capability of the sample toward photocatalytic reactions was assessed by using MB solution as a representative of organic pollutant dye. 73% photodegradation efficiency and 0.0045 min-1 rat constant under visible light radiation were the results of the photocatalytic test, proving the fact that the synthesized SnS2 nanoflakes were highly efficient as visible light-responsive photocatalysts. Mott-Schottky analysis of the sample showed that the synthesized SnS2 was n-type and had a flat band potential of -0.02 eV (vs. NHE). Finally, band structure positions, obtained by Mott-Schottky and DRS results, of SnS2 nanoflakes suggested that the photogenerated holes and hydroxyl radicals as active species were responsible for MB mineralization.

Conflict of interest

The authors declare that they have no conflict of interest.

Acknowledgments

The authors express their gratitude for the assistance provided by the Iran Nanotechnology Initiative Council in supporting this research endeavor.

References

1. Yin Z, Han M, Hu Z, Feng L, Liu Y, Du Z, Zhang L. Peroxymonosulfate enhancing visible light photocatalytic degradation of bezafibrate by Pd/g-C3N4 catalysts: The role of sulfate radicals and hydroxyl radicals. Chemical Engineering Journal. 2020;390:124532.

2. Rafiq A, Ikram M, Ali S, Niaz F, Khan M, Khan Q, Maqbool M. Photocatalytic degradation of dyes using semiconductor photocatalysts to clean industrial water pollution. Journal of Industrial and Engineering Chemistry. 2021;97:111-28.

3. Gusain R, Gupta K, Joshi P, Khatri OP. Adsorptive removal and photocatalytic degradation of organic pollutants using met-

al oxides and their composites: A comprehensive review. Advances in Colloid and Interface Science. 2019;272:102009.
4. Saravanan R, Gracia F, Stephen A. Basic Principles, Mechanism, and Challenges of Photocatalysis. Nanocomposites for Visible Light-induced Photocatalysis: Springer International Publishing; 2017. p. 19-40.
5. Xiao M, Wang Z, Lyu M, Luo B, Wang S, Liu G, et al. Hollow Nanostructures for Photocatalysis: Advantages and Challenges. Advanced Materials. 2018;31(38).
6. Zarezadeh K, Sheibani S, Ataie A. Photocatalytic and antibacterial characteristics of decorated polyester textile with ceramic nanoparticles of cobalt ferrite. Ceramics International. 2023;49(12):20104-17.
7. Zare A, Saadati A, Sheibani S. Modification of a Z-scheme ZnO-CuO nanocomposite by Ag loading as a highly efficient visible light photocatalyst. Materials Research Bulletin. 2023;158:112048.
8. Alikarami S, Soltanizade A, Rashchi F. Synthesis of CdS–SnS photocatalyst by chemical co-precipitation for photocatalytic degradation of methylene blue and rhodamine B under irradiation by visible light. Journal of Physics and Chemistry of Solids. 2022;171:110993.
9. Zhang G, Guan Z, Yang J, Li Q, Zhou Y, Zou Z. Metal Sulfides for Photocatalytic Hydrogen Production: Current Development and Future Challenges. Solar RRL. 2022;6(10).
10. She H, Sun Y, Li S, Huang J, Wang L, Zhu G, Wang Q. Synthesis of non-noble metal nickel doped sulfide solid solution for improved photocatalytic performance. Applied Catalysis B: Environmental. 2019;245:439-47.
11. Tian Y, Zhang J, Yang X, Jia D. Facile One-Pot Synthesis and Enhanced Photocatalytic Performances of Ternary Metal Sulfide Composite g- C_3N_4/Cu_3SnS_4. European Journal of Inorganic Chemistry. 2022;2022(19).
12. Zhang G, Du X, Wang Y, Wang H, Wang W, Fu Z. Controllable synthesis of SnS_2 nanostructures with high adsorption and photocatalytic activities. Materials Science in Semiconductor Processing. 2017;64:77-84.
13. Liu J-H, Huang G-F, Huang W-Q, Miao H, Zhou B-X. Morphology-controlled SnS2 nanostructures synthesized by refluxing method with high photocatalytic activity. Materials Letters. 2015;161:480-3.
14. Zhang YC, Li J, Zhang M, Dionysiou DD. Size-Tunable Hydrothermal Synthesis of SnS_2 Nanocrystals with High Performance in Visible Light-Driven Photocatalytic Reduction of Aqueous Cr(VI). Environmental Science & amp; Technology. 2011;45(21):9324-31.
15. Kovacic M, Papac J, Kusic H, Karamanis P, Loncaric Bozic A. Degradation of polar and non-polar pharmaceutical pollutants in water by solar assisted photocatalysis using hydrothermal TiO_2-SnS_2. Chemical Engineering Journal. 2020;382:122826.
16. Saadati A, Sheibani S. Insight into the adsorption and photocatalytic properties of in-situ synthesized g-C_3N_4/SnS_2 nanocomposite. Ceramics International. 2022;48(20):30294-306.
17. Zhang F, Zhang Y, Zhou C, Yang Z, Xue H, Dionysiou DD. A new high efficiency visible-light photocatalyst made of SnS_2 and conjugated derivative of polyvinyl alcohol and its application to Cr(VI) reduction. Chemical Engineering Journal. 2017;324:140-53.
18. Lei Y, Song S, Fan W, Xing Y, Zhang H. Facile Synthesis and Assemblies of Flowerlike SnS_2 and In3+-doped SnS_2: Hierarchical Structures and Their Enhanced Photocatalytic Property. The Journal of Physical Chemistry C. 2009;113(4):1280-5.
19. Huang Q, Yu J, Cao S, Cui C, Cheng B. Efficient photocatalytic reduction of CO_2 by amine-functionalized g-C_3N_4. Applied Surface Science. 2015;358:350-5.
20. Mohtar SS, Aziz F, Ismail AF, Sambudi NS, Abdullah H, Rosli AN, Ohtani B. Impact of Doping and Additive Applications on Photocatalyst Textural Properties in Removing Organic Pollutants: A Review. Catalysts. 2021;11(10):1160.
21. Saadati A, Sheibani S. Nitrogen-doped carbon dot impregnated g-C_3N_4/SnS_2 nanocomposite as an efficient mediator and co-catalyst for enhanced photocatalytic degradation and water splitting. Journal of Alloys and Compounds. 2023;947:169594.
22. Adeyemi JO, Onwudiwe DC. SnS_2 and SnO_2 Nanoparticles Obtained from Organotin(IV) Dithiocarbamate Complex and Their Photocatalytic Activities on Methylene Blue. Materials (Basel). 2020;13(12):2766.
23. Sharma K, Patial S, Singh P, Khan AAP, Saini V, Nadda AK, et al. Strategies and perspectives of tailored SnS_2 photocatalyst for solar driven energy applications. Solar Energy. 2022;231:546-65.
24. Park S, Park J, Selvaraj R, Kim Y. Facile microwave-assisted synthesis of SnS_2 nanoparticles for visible-light responsive photocatalyst. Journal of Industrial and Engineering Chemistry. 2015;31:269-75.
25. Zhang YC, Du ZN, Li KW, Zhang M. Size-controlled hydrothermal synthesis of SnS_2 nanoparticles with high performance in visible light-driven photocatalytic degradation of aqueous methyl orange. Separation and Purification Technology. 2011;81(1):101-7.
26. Bora LV, Mewada RK. Visible/solar light active photocatalysts for organic effluent treatment: Fundamentals, mechanisms and parametric review. Renewable and Sustainable Energy Reviews. 2017;76:1393-421.
27. Srivind J, Nagarethinam VS, Suganya M, Balamurugan S, Usharani K, Balu AR. NiO coupled SnS_2 nanoparticles with improved magnetic and photocatalytic performance against the degradation of organic dyes without N N double bond. Vacuum. 2019;163:373-83.
28. Feng J, Sun Y, Mu J, Chen L, Han T, Miao H, et al. Microwave-assistant synthesis of Au/SnS_2 nanoflowers as improved visible-light responsive photocatalysts. Materials Letters. 2019;236:534-7.
29. Qiang T, Chen L, Xia Y, Qin X. Dual modified MoS_2/SnS_2 photocatalyst with Z-scheme heterojunction and vacancies defects to achieve a superior performance in Cr (VI) reduction and dyes degradation. Journal of Cleaner Production. 2021;291:125213.
30. Govindan V, Kashinath L, Joseph Daniel D, Sankaranarayanan K. Sol–gel mediated microwave synthesis of pure, La and Zr doped SnS_2 nanoflowers an efficient photocatalyst for the degradation of methylene blue. Journal of Materials Science: Materials in Electronics. 2019;30(8):7963-73.
31. Ruan Q, Miao T, Wang H, Tang J. Insight on Shallow Trap States-Introduced Photocathodic Performance in n-Type Polymer Photocatalysts. J Am Chem Soc. 2020;142(6):2795-802.
32. Ahmad N, Kuo C-FJ, Mustaqeem M, Sangili A, Huang C-C, Chang H-T. Synthesis of novel Type-II $MnNb_2O_6$/g-C_3N_4 Mott-Schottky heterojunction photocatalyst: Excellent photocatalytic performance and degradation mechanism of fluoroquinolone-based antibiotics. Chemosphere. 2023;321:138027.
33. Giannakopoulou T, Papailias I, Todorova N, Boukos N, Liu Y, Yu J, Trapalis C. Tailoring the energy band gap and edges' potentials of g-C_3N_4 /TiO_2 composite photocatalysts for NOx removal. Chemical Engineering Journal. 2017;310:571-80.
34. Yulizar Y, Eprasatya A, Bagus Apriandanu DO, Yunarti RT. Facile synthesis of ZnO/$GdCoO_3$ nanocomposites, characterization and their photocatalytic activity under visible light illumination. Vacuum. 2021;183:109821.